applied sciences

MDPI

Article

Enhanced Performance of Inverted Perovskite Solar Cells Employing NiO_x and Cu-Doped NiO_x Nanoparticle Hole Transport Layers

Ponmudi Selvan Thiruchelvan [1], Chien-Chih Lai [2,3] and Chih-Hung Tsai [3,*]

[1] Department of Physics, Hindustan Institute of Technology and Science, Chennai 603103, Tamilnadu, India; lonelyselva@gmail.com
[2] Department of Physics, National Dong Hwa University, Hualien 97401, Taiwan; cclai@gms.ndhu.edu.tw
[3] Department of Opto-Electronic Engineering, National Dong Hwa University, Hualien 97401, Taiwan
* Correspondence: cht@mail.ndhu.edu.tw; Tel.: +886-3-890-3199

Abstract

In this study, p-type NiO_x and Cu-doped NiO_x nanoparticles (NPs) were synthesized by a simple chemical precipitation method and used as hole transport layers (HTLs) for inverted perovskite solar cells (PSCs). The microstructural property, surface morphology, elemental composition, optical property, charge recombination, and surface topography of the NiO_x and Cu-NiO_x HTLs were comprehensively characterized. The results showed that the NiO_x and Cu-NiO_x NPs were uniformly coated on the substrates without pinholes or voids. Cu incorporation into NiO_x did not change its crystalline nature and considerably improved its electrical conductivity. The Cu-NiO_x HTLs exhibited superior photoluminescence quenching and the least lifetime decay, which indicated that Cu-NiO_x exhibited higher charge transport than NiO_x HTLs. The fabricated PSC performances were further analyzed using current density–voltage characteristics, external quantum efficiency, and electrochemical impedance spectroscopy. The PSCs with PEDOT:PSS, NiO_x, and 2% Cu-NiO_x HTLs exhibited power conversion efficiencies of 11.93%, 13.72%, and 15.54%, respectively. The 2% Cu-NiO_x HTL-based device showed the best performance compared with the PEDOT:PSS- and NiO_x-based devices. Academic Editors: Chunyang Zhang, Dou Zhang

Keywords: perovskite solar cells; hole transport layer; nickel oxide; copper doping; nanoparticles

check for updates

Academic Editors: Chunyang Zhang and Dou Zhang

Received: 5 October 2025
Revised: 23 October 2025
Accepted: 24 October 2025
Published: 27 October 2025

Citation: Thiruchelvan, P.S.; Lai, C.-C.; Tsai, C.-H. Enhanced Performance of Inverted Perovskite Solar Cells Employing NiO_x and Cu-Doped NiO_x Nanoparticle Hole Transport Layers. *Appl. Sci.* **2025**, *15*, 11449. https://doi.org/10.3390/app152111449

Copyright: © 2025 by the authors. Licensee MDPI, Basel, Switzerland. This article is an open access article distributed under the terms and conditions of the Creative Commons Attribution (CC BY) license (https://creativecommons.org/licenses/by/4.0/).

1. Introduction

Organic and inorganic metal halide perovskites have emerged as pivotal materials in optoelectronic applications due to their high charge-carrier mobility, strong light absorption, and tunable bandgap. Moreover, they have the potential to expand their applications into diverse fields such as photocatalysis [1], energy storage [2], and advanced computing and memory (memristors) [3]. Over the past decade, perovskite solar cells (PSCs) have attracted significant attention owing to their rapidly increasing power conversion efficiency and potential for commercialization [4–6]. Structurally, PSCs are generally categorized into two configurations: conventional (n–i–p) and inverted (p–i–n). Although conventional PSCs are efficient, they are highly susceptible to hysteresis and thermal instability and are expensive. Inverted PSCs exhibit limited hysteresis and excellent stability but inferior PCE. Nevertheless, inverted PSCs have attracted considerable research interest because of their simple fabrication processes and suitability for use in flexible devices due to their low-temperature processing. The performance of inverted PSCs can be improved through hole

transport layer (HTL) engineering. The requirements of PSCs are high optical transparency, hole mobility, and energy alignment with the perovskite layers.

In inverted PSCs, poly(3,4-(ethylenedioxy)thiophene)/poly(styrene sulfonate) (PEDOT:PSS) HTLs are common. However, these HTLs are hygroscopic and acidic, which severely affects PSC stability. Therefore, metal oxides are an ideal candidate for replacing organic HTLs. NiO_x is the most widely studied HTL material because of its excellent p-type semiconducting property, high transparency, and numerous deposition methods. In 2014, Jeng et al. first introduced NiO_x HTLs in PSCs as a replacement for PEDOT:PSS [7]. Several researchers have since developed NiO_x thin films for PSCs by using various methods such as those using the sol–gel process, combustion, nanoparticle (NP) ink, chemical bath deposition, electrodeposition, spray pyrolysis, sputtering, electron-beam physical vapor deposition process, and pulsed-laser deposition [8–23]. Low-temperature fabrication methods are attractive because they are suitable for fabricating flexible devices. NiO_x HTLs are typically prepared using a low-temperature (150 °C) combustion method. NiO_x HTLs prepared from NP ink are easy to fabricate and exhibit higher crystallinity than those prepared with other techniques. This method can be readily adapted for the doping of other metals to improve the hole mobility of the NiO_x layer. This improvement is crucial because NiO_x is limited because of its electrical property and exhibits lower hole mobility, valence band maximum, and more surface defects than (PEDOT:PSS) HTLs. Techniques such as doping and surface modification have been proposed to improve the conductivity and charge collection of NiO_x HTLs [24–27]. Metal doping is the best surface modification approach for improving the electrical properties of NiO_x HTLs. Many researchers have reported doping NiO_x with metals such as Li, Cu, Mg, Co, Cs, and Fe [28–32].

Cu doping has attracted considerable research attention because of its high carrier concentration, mobility, and work function [33]. Several reports have demonstrated PCEs exceeding 23% in inverted perovskites solar cells through strategies such as multication incorporation at the A-site, the use of two-dimensional (2D) perovskites, and interface engineering at both the HTL and the ETL [34,35]. In this work, we focus on the incorporation of Cu at the Ni site to enhance the electrical properties and overall device performance by modifying the HTL without any heating or annealing during the fabrication process, except for the perovskite film. We fabricated inverted PSCs with presynthesized NiO_x NP and Cu-doped NiO_x (Cu-NiO_x) NP HTLs. The device structure was Glass/FTO/NiO_x or Cu-NiO_x or PEDOT:PSS/perovskite/PCBM/BCP/Ag, as shown in Figure 1a, and its equivalent energy level diagram is displayed in Figure 1b. A simple chemical precipitation technique was used to prepare NiO_x NPs. The synthesized NPs were characterized through X-ray diffraction (XRD), X-ray photoelectron spectroscopy (XPS), field emission scanning electron microscopy (FESEM), ultraviolet (UV)–visible (Vis) spectroscopy, photoluminescence (PL) spectroscopy, and atomic force microscopy (AFM). The performance of the fabricated device was characterized using current density–voltage (J–V) analysis, electrochemical impedance spectroscopy (EIS), and external quantum efficiency (EQE). The fabricated Cu-NiO_x PSCs exhibited improved performance. The PSCs fabricated using 2% Cu-NiO_x NP inks, with a PCE of 15.54%, exhibited the highest efficiency. The device fabricated using pristine NiO_x and PEDOT:PSS exhibited PCEs of 13.72% and 11.93%, respectively.

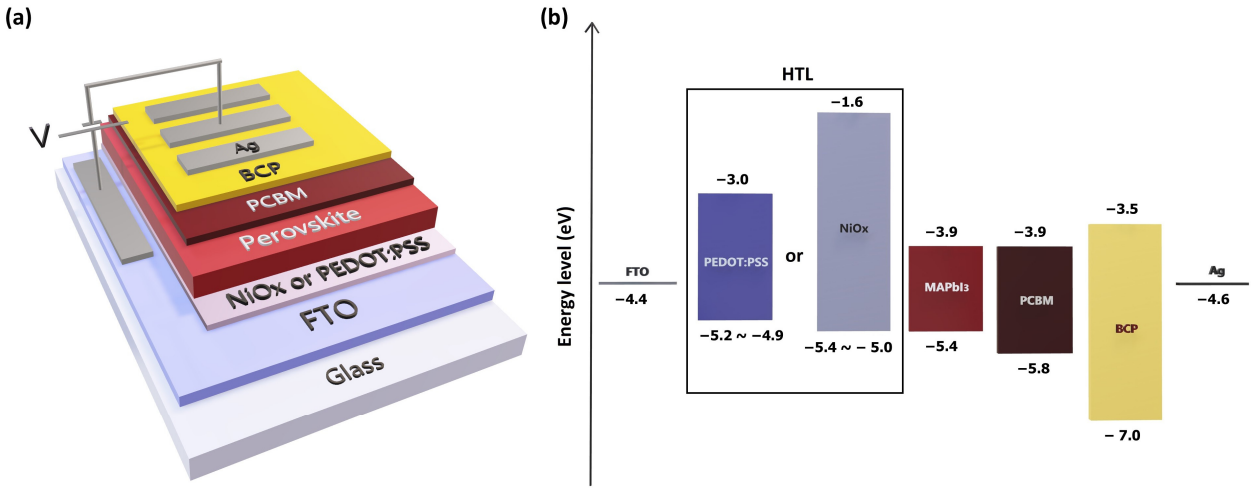

Figure 1. (**a**) Device structure and (**b**) energy level diagram of fabricated inverted PSCs.

2. Experimental Details

2.1. Synthesis of NiO and Cu-Doped NiO NPs

First, 0.4 M nickel nitrate hexahydrate ($Ni(NO_3)_2$ $6H_2O$) (CHONEYE PURE CHEMICALS, Miaoli County, Taiwan, Purity > 98%) was dissolved in deionized (DI) water to obtain a green solution. Then, 10 M sodium hydroxide (NaOH) was added dropwise till the solution reached a pH of 10. The precipitate was stirred for 30 min, centrifuged at 16,000 rpm for 10 min, and washed with DI water three times. The green powders were dried at 80 °C overnight and calcined at 270 °C for 2 h at a 5 °C/min ramping rate. Finally, NiO_x NPs in the form of black powder were obtained. The NPs were dispersed in DI water at a 20 mg/mL concentration. For Cu doping, various mole percentages of nickel nitrate were replaced by Copper(II) nitrate trihydrate $Cu(NO_3)_2$ $3H_2O$ (CHONEYE PURE CHEMICALS, Miaoli County, Taiwan, Purity > 98%). Other procedures were the same as those for the undoped NiO_x NPs.

2.2. PSC Device Fabrication

The schematic of PSC device fabrication is represented in Figure 2. FTO substrates (Ruilong Optoelectronics Co., Ltd, Miaoli County, Taiwan) were patterned and cleaned in an ultrasonic bath using detergent, acetone, and isopropyl alcohol (IPA) for 10 min. Then, the substrates were dried using a nitrogen gun and UV–ozone treated for 15 min. The HTL production method was as follows: NiO_x (or Cu-NiO_x) NP ink was spin-coated onto the FTO substrates at a speed of 3000 rpm for 30 s. We also fabricated devices with a PEDOT:PSS HTL for comparison. The PEDOT:PSS (UNI-ONWARD Corp, New Taipei City, Taiwan) was spin-coated at 4000 rpm for 30 s and annealed at 140 °C for 10 min. Subsequently, the perovskite active layer was produced through the following procedures: 1.4 M MAI (UNI-ONWARD Corp, New Taipei City, Taiwan) and 1.4 M PbI_2 (UNI-ONWARD Corp, New Taipei City, Taiwan) were dissolved in a mixed solvent of GBL/DMSO in a 7:3 ratio. The perovskite solution was stirred at 60 °C overnight and filtered using a 0.45 µm PTFE syringe filter before deposition. The solution was spin-coated onto the FTO/NiO_x substrates at 1000 rpm for 15 s and 5000 rpm for 25 s. Toluene was used as an antisolvent and was added exactly 5 s before the end of the second step. The substrates were annealed at 100 °C for 10 min. The electron transport layer (ETL) production process was as follows: 20 mg/mL of phenyl-C61-butyric acid methyl ester (PCBM) in 1,4-dichlorobenzene was spin-coated on the substrates at 2000 rpm for 30 s, and a saturated solution of BCP in methanol was spin-coated at 6000 rpm for 30 s. No annealing

process was performed during fabrication, except for the perovskite film. Finally, a Ag electrode was evaporated through thermal evaporation.

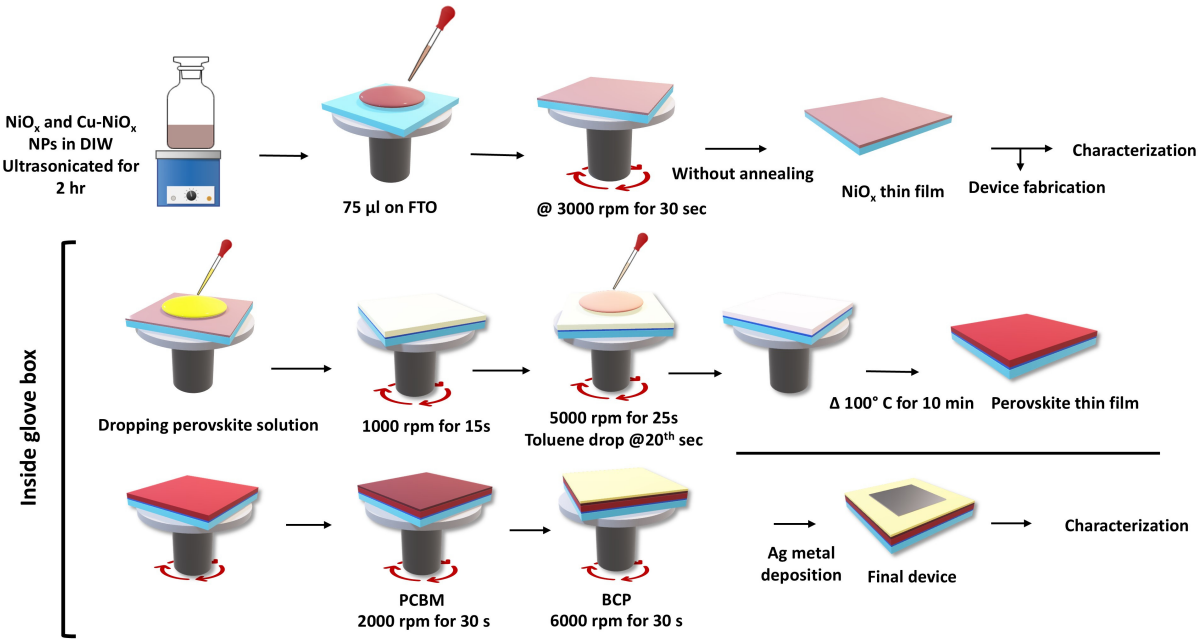

Figure 2. Schematic diagram of device fabrication.

2.3. Characterization

NiO_x and Cu-NiO_x were characterized through XRD (Rigaku D/Max-2500V, Rigaku Corp, Tokyo, Japan); their surface morphology was observed through FESEM (JEOL JSM-7000F, JEOL Inc., Tokyo, Japan), and their surface topography was measured through AFM (AutoProbe CP, Thermomicroscopes, Sunnyvale, CA, USA). Moreover, elemental analysis was performed through XPS (Thermo K-Alpha, Thermo Fisher Scientific, Waltham, MA, USA). UV-Vis absorption and transmission were measured through a UV-Vis spectrophotometer (Jasco V-650, Jasco, Tokyo, Japan). PL and lifetime measurements were performed using a solid-state laser (λ = 405 nm, PDL 800-D, PICOQUANT) equipped with a homemade laser scanning confocal microscope and a spectrometer equipped with a thermoelectrically cooled charge-coupled detector (DV420A-BU2, Andor, Belfast, Northern Ireland). The performance of the fabricated PSC device was analyzed using J–V curves (CH 6116D, CH Instruments, Bee Cave, TX, USA), EQE (QE-R, Enlitech, Kaohsiung, Taiwan), and EIS. The J–V characteristics of the PSCs were measured under the illumination of a simulated AM 1.5G solar spectrum from a 550-W Xe lamp solar simulator (Abet Technologies Sun 3000 Class AAA, Abet Technologies, Milford, CT, USA).

3. Results and Discussion

3.1. Chemical Reaction Mechanism of NiO_x and Cu-NiO_x NPs

The NiO_x and Cu-NiO_x NPs were synthesized using a simple chemical precipitation method according to procedures reported in studies [36–42] with some modifications (see details in the experimental section). We synthesized pristine NiO_x NPs and 2%, 4%, and 8% Cu-NiO_x NPs. HTL development using simple synthesis methods is promising for the large-scale industrial production of PSCs. The chemical reaction mechanism of nonstoichiometric NiO_x NPs and Cu-NiO_x NPs is expressed in Equations (1)–(4), respectively.

$$Ni(NO)_3 + NaOH \rightarrow Ni(OH)_2 \downarrow + Na(NO_3)_2 \quad (1)$$

$$Ni(OH)_2 \xrightarrow{270\ ^{\circ}C} NiO_x + H_2O \quad (2)$$

$$Ni(NO)_3 + Cu(NO)_3 + NaOH \rightarrow Ni(OH)_2 \downarrow + Cu(OH)_2 \downarrow + Na(NO_3)_2 \quad (3)$$

$$Ni(OH)_2 + Cu(OH)_2 \xrightarrow{270\ ^{\circ}C} Cu - doped\ NiO_x + H_2O \quad (4)$$

The calcination temperature was set at 270 °C to ensure the thermal decomposition of $Ni(OH)_2$ to nonstoichiometric NiO_x NPs. However, $Ni(OH)_2$ cannot completely decompose to NiO at a temperature lower than the calcination temperature of 270 °C. Because $Ni(OH)_2$ is electrically insulated, it cannot be easily dispersed in solvents. If the calcination temperature exceeds 270 °C, the particle size increases. Both cases are not suitable for making an effective HTL for PSCs.

3.2. Characterization of the HTLs

XRD patterns for pristine NiO_x and various percentages of Cu-NiO_x NPs are illustrated in Figure 3. The diffraction peaks at 2θ were approximately 37°, 43°, and 62°, which corresponded to the (hkl) planes of (111), (002), and (022), respectively. Two other small peaks were obtained at approximately 75° and 79°, which corresponded to the (113) and (222) planes, respectively. The (002) peak domination in all the NPs and broad peaks indicated the presence of small crystals in the synthesized NPs. The crystallite size calculated using the Debye–Scherrer formula was approximately 4–6 nm. The XRD data is presented in Table 1. The XRD results were consistent with the values of the International Center for Diffraction Data (reference number: 98-000-5229), which confirmed the existence of the cubic NiO_x phase. No other peaks related to metallic copper or copper oxide were observed, which revealed that the incorporation of Cu into nickel oxide did not change its crystal structure [43].

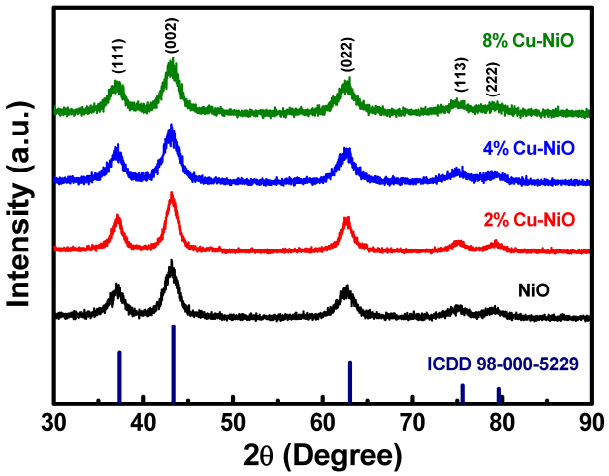

Figure 3. XRD patterns of the NiO_x and various concentration of Cu-NiO_x nanoparticles.

The optical properties were studied using UV-Vis spectroscopy. We measured the absorbance spectra of equally concentrated NiO_x and Cu-NiO_x NPs dispersed in DI water (Figure 4) in the wavelength range from 300 to 800 nm. The absorbance increased with an increase in the Cu concentration. The optical bandgaps were calculated using the standard Tauc plot method. The bandgap values were 3.8, 3.74, 3.71, and 3.66 eV for undoped NiO_x, 2%, 4%, and 8% Cu-NiO_x NPs, respectively. The bandgap values of synthesized NPs decreased with an increase in the Cu concentration. The incorporation of Cu atoms slightly narrowed the bandgap. The transmittance spectra of spin-coated NiO_x and Cu-NiO_x NPs on glass is illustrated in Figure 5, which revealed more than 85% of transmission in the

visible region. The transmittance value decreased with an increase in the Cu concentration because of the narrowing bandgap.

Table 1. Microstructural properties of NiO_x and Cu-NiO_x nanoparticles.

Sample	2θ	(hkl)	Interplanar Distance (Å)	FWHM (β) (radians)	Crystallite Size (D) (nm)	Dislocation Density ($1/D^2$) ($\times 10^{16}$)	Microstrain (β/4tanθ)	Lattice Parameter (a)
NiO_x	37	(111)	2.43	0.03	4.94	4.12	1.27	4.21
	43.09	(002)	2.1	0.04	4.73	4.49	1.15	4.2
	62.54	(022)	1.49	0.04	4.52	4.92	0.85	4.21
2% Cu-NiO_x	37.09	(111)	2.43	0.03	6.51	2.37	0.96	4.2
	43.16	(002)	2.1	0.03	5.67	3.13	0.96	4.2
	62.59	(022)	1.49	0.03	6.25	2.57	0.62	4.2
4% Cu-NiO_x	36.96	(111)	2.44	0.03	4.91	4.17	1.28	4.22
	43.07	(002)	2.11	0.04	4.21	5.65	1.29	4.21
	62.55	(022)	1.49	0.04	4.06	6.07	0.95	4.2
8% Cu-NiO_x	36.96	(111)	2.44	0.04	4.53	4.88	1.39	4.22
	43.11	(002)	2.1	0.04	4.28	5.49	1.27	4.2
	62.57	(022)	1.49	0.05	3.98	6.34	0.97	4.2
ICDD 98-000-5229	37.25	(111)	2.42					
	43.28	(002)	2.09					
	62.86	(022)	1.48					

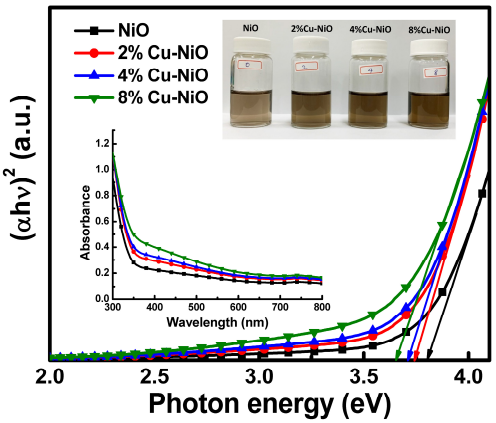

Figure 4. The optical bandgap, absorbance spectra, and photograph of NiO_x and various concentration of Cu-NiO_x nanoparticles.

The surface morphologies of NiO_x and various percentages of Cu-NiO_x NPs were observed through FESEM. Figure 6 clearly reveals that the NPs completely covered the substrate, and no pinholes or voids occurred, which confirmed the presence of some nanoclusters in the 4% and 8% Cu-NiO_x NP films. The size of the nanoclusters increased with an increase in the doping concentration of Cu. The conversion of $Ni(OH)_2$ to NiO_x occurred in the temperature range 250–305 °C, but the conversion of $Cu(OH)_2$ to CuO occurred from 150 °C, which resulted in the formation of these small nanoclusters. So far, the formation of these clusters because of copper doping has not been reported. The FESEM images of NiO_x and 2% Cu-NiO_x were similar, and they almost completely dispersed in DI water. In similar studies, the thickness of the HTL was reported to be approximately 50 nm, which is typically sufficient to ensure uniform coverage and efficient charge transport without increasing series resistance [44]. Therefore, they were selected for device fabrication.

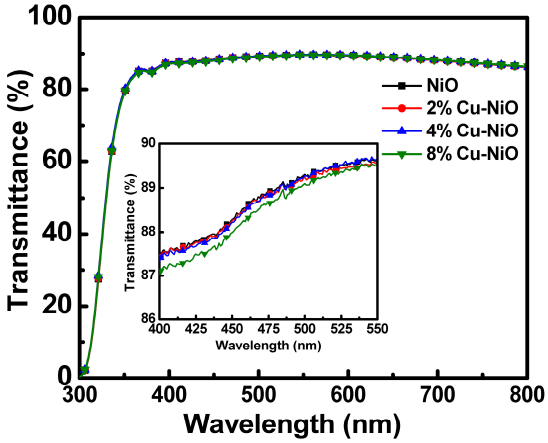

Figure 5. Transmittance spectra of NiO_x and various concentration of Cu-NiO_x spin-coated thin films.

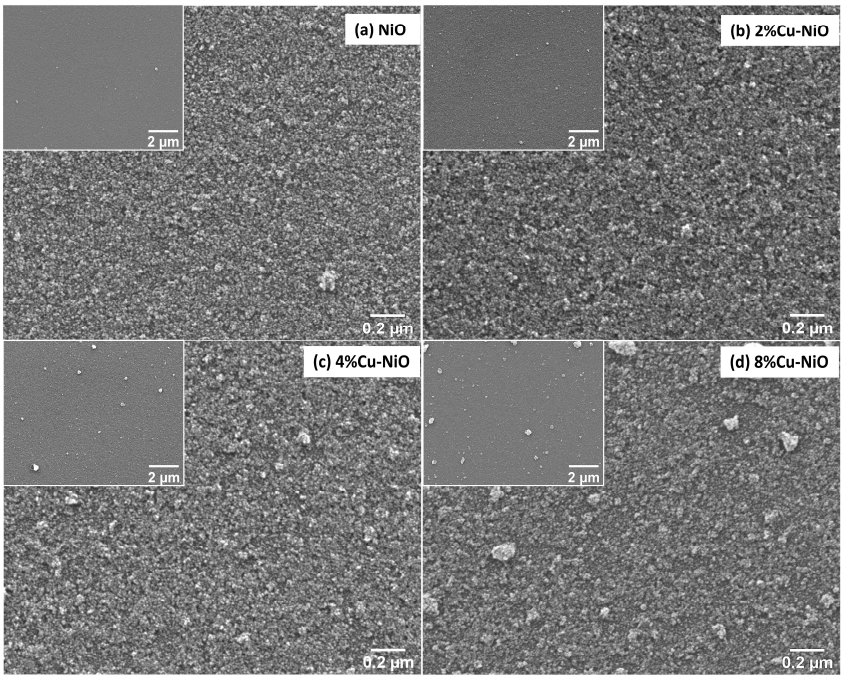

Figure 6. FESEM images of (**a**) NiO_x, (**b**) 2%, (**c**) 4%, and (**d**) 8% Cu-NiO_x spin-coated thin films.

XPS was performed to examine the elemental composition of NiO_x NPs and 2% Cu-NiO_x films. The XPS spectra of the Ni 2p, O 1s, and Cu 2p core level are illustrated in Figure 7. The Ni 2p spectra consisted of two peaks, namely, the main peak and the shoulder peak. The deconvoluted peaks at 853, 856, and 858 eV corresponded to NiO (Ni^{2+}), Ni_2O_3 (Ni^{3+}), and NiOOH, respectively. The Ni^{3+} ions confirmed the presence of Ni vacancies in the film, which rendered the film a p-type semiconductor. The peak at 861 eV was attributed to the modification of the NiO structure [45,46]. There was no significant change in the Ni 2p peaks between the NiO_x and Cu-NiO_x thin films. The O 1s spectra exhibited three peaks at 529, 531, and 533 eV, which corresponded to NiO (Ni^{2+}), Ni_2O_3 (Ni^{3+}), and NiOOH ions, respectively. In Cu 2p spectra, the peaks located at 933 and 953 eV corresponded to Cu $2p_{3/2}$ and Cu $2p_{1/2}$ transitions, respectively. The Cu^{2+} peak was dominant in Cu $2p_{3/2}$ spectra, whereas the Cu^{+} peak was not significant [47]. The surface topography of NiO_x and 2% Cu-NiO_x NP thin films was investigated through AFM. Figure 8 displays the AFM images of NiO_x and 2% Cu-NiO_x NP thin films. The average root-mean-square roughness values of the NiO_x and 2% Cu-NiO_x NPs films were 4.068 ± 1.067 and 3.527 ± 0.9376 nm, respectively. The roughness decreased with Cu doping, which was consistent with reports.

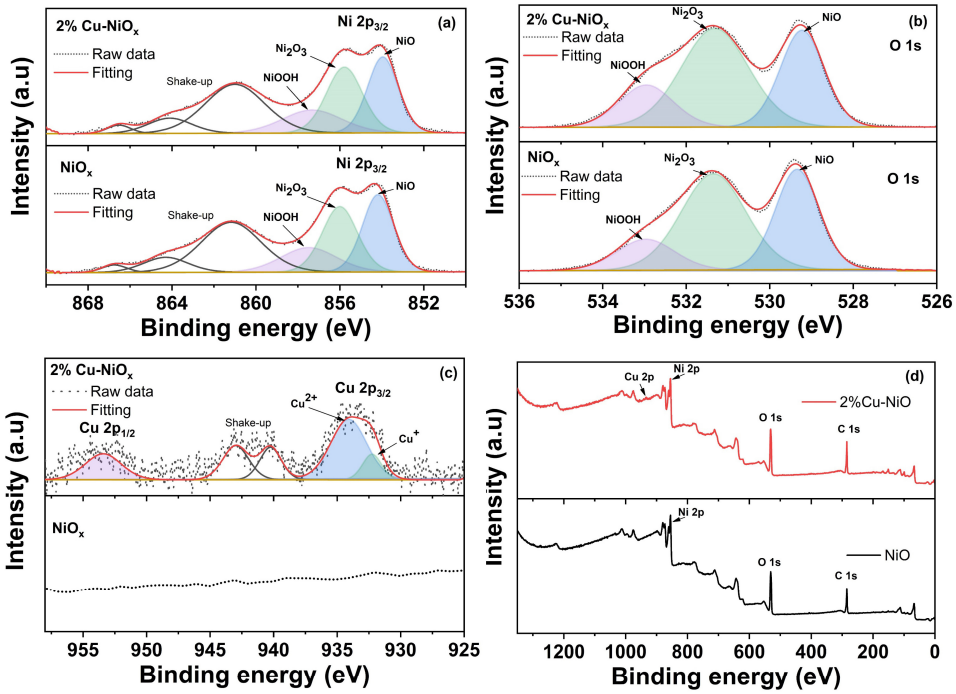

Figure 7. XPS spectra of (**a**) Ni 2p, (**b**) O 1s, (**c**) Cu 2p, and (**d**) survey scan for NiO_x and 2% Cu-NiO_x thin films.

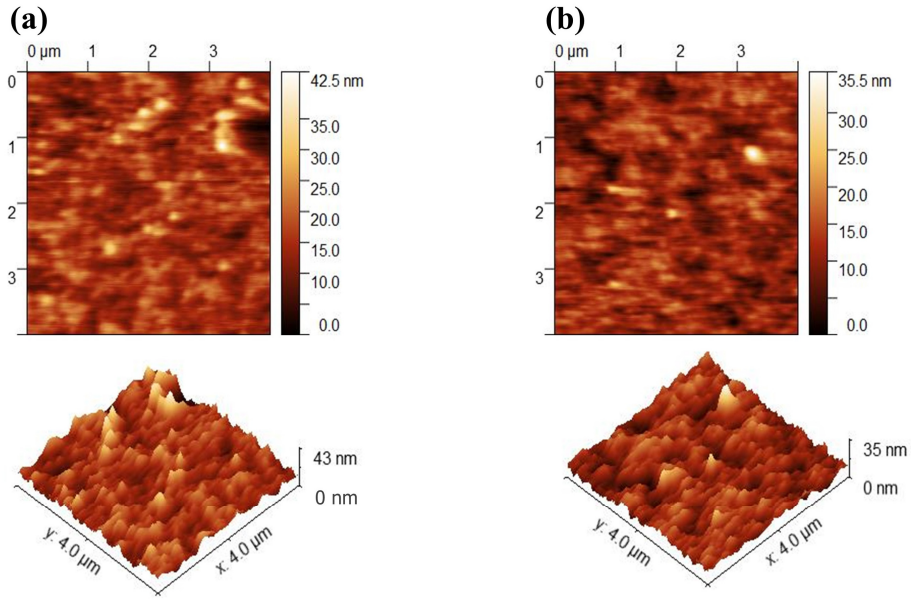

Figure 8. AFM images of (**a**) NiO_x and (**b**) 2% Cu-NiO_x thin films.

PL and time-resolved PL (TRPL) were used to evaluate charge extraction and recombination from the devices. Typically, PL quenching and a short PL lifetime are expected for perovskites in contact with charge transport layers. We measured the PL spectra and the TRPL profile of the perovskite layers deposited on various HTLs (Figure 9). The PL quenching was better for the perovskite film deposited on Cu-NiO_x than for that on pristine NiO_x, which indicated that Cu incorporation in NiO_x improved the charge extraction property from the perovskite film. The TRPL profile was measured through time-correlated single-photon counting to analyze charge dynamics. PL lifetime decay tails were fitted with biexponential fitting function $y = y_0 + A_1 e^{-(x-x_0)/\tau_1} + A_2 e^{-(x-x_0)/\tau_2}$, where ($\tau_1$) is related to the diffusion of photogenerated excitons into defects, and (τ_2) is related to intrinsic electron–hole recombination. The average PL lifetime value was calculated using the

formula $\tau_{avg} = \left(\Sigma_i A_i \tau_i^2\right) / \left(\Sigma_i A_i \tau_i\right)$. The obtained fitting values are summarized in Table 2. The PL lifetime for the perovskite film deposited on Cu-NiO_x was shorter than that of pristine NiO_x, which indicates higher efficient charge transfer in Cu-NiO_x.

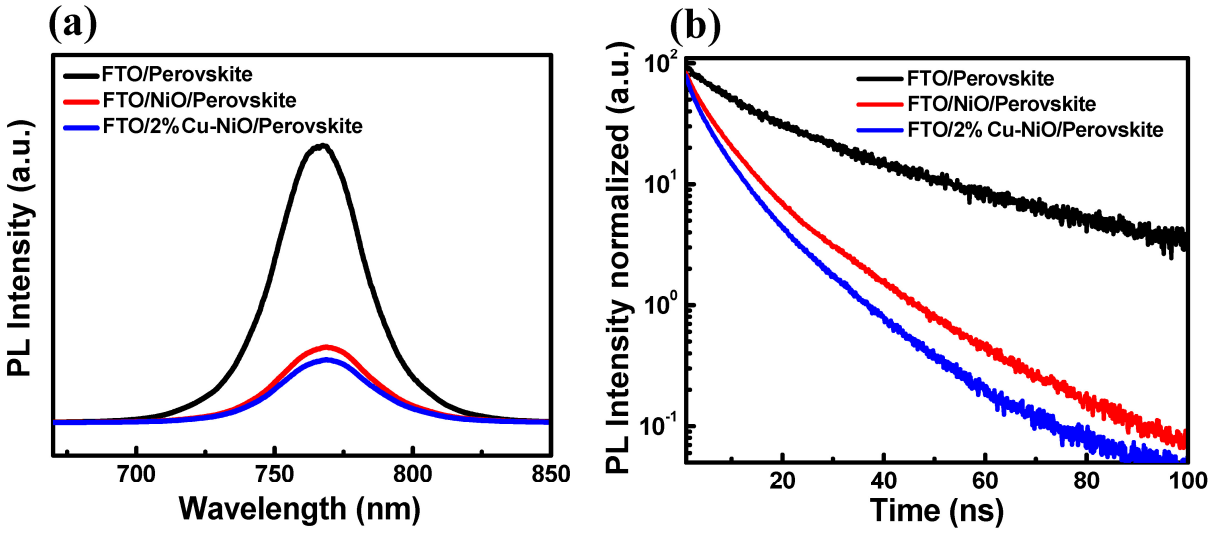

Figure 9. (**a**) Photoluminescence spectra and (**b**) time-resolved PL spectra for perovskite films on different HTLs.

Table 2. Summary of the PL lifetime parameters from the fitting curves of the PL decay.

Sample	A_1 (%)	τ_1 (ns)	A_2 (%)	τ_2 (ns)	τ_{avg} (ns)
FTO/PSK	61.8	9.6	38.2	37.6	29.4
FTO/NiO_x/PSK	64.9	3.3	35.1	11.4	8.6
FTO/2% Cu-NiO_x/PSK	55.9	2.2	44.1	8.6	7.0

3.3. Characterization of the PSC Devices

The J–V curve, EQE, and EIS analyses were performed to investigate the PSC device performance of the synthesized NiO_x and 2% Cu-NiO_x NP HTLs. The device structure of the inverted PSCs was Glass/FTO/NiO_x or Cu-NiO_x or PEDOT:PSS/perovskite/PCBM/BCP/Ag. We also fabricated PSCs with a PEDOT:PSS HTL for comparison. The J–V analysis was first performed on the devices to investigate the effects of Cu doping in NiO_x NP HTLs on the short-circuit current density (J_{SC}), open-circuit voltage (V_{OC}), fill factor (FF), and PCE of the PSC device. The J–V curves of fabricated inverted PSCs with PEDOT:PSS, NiO_x, and 2% Cu-NiO_x HTLs are displayed in Figure 10. Both NiO_x and 2% Cu-NiO_x exhibited better performance than the PEDOT:PSS HTL devices. The detailed device parameters are listed in Table 3. The 2% Cu-NiO_x device exhibited the highest J_{SC} value of 20.57 mA/cm^2, whereas the PEDOT:PSS and pristine NiO_x devices exhibited J_{SC} values of 18.83 and 18.66 mA/cm^2, respectively. The J_{SC} value was higher in the Cu-based device than that in the pristine NiO_x device. This phenomenon was attributed to the increased electrical conductivity and better energy alignment of the HTL to the perovskite layer because of the incorporation of Cu in nickel oxide. The 2% Cu-NiO_x device exhibited a V_{OC} of 1.026, an FF of 0.74, and a PCE of 15.54%. The 2% Cu-NiO_x NP-based device showed the best performance compared with the pristine NiO_x and PEDOT:PSS devices.

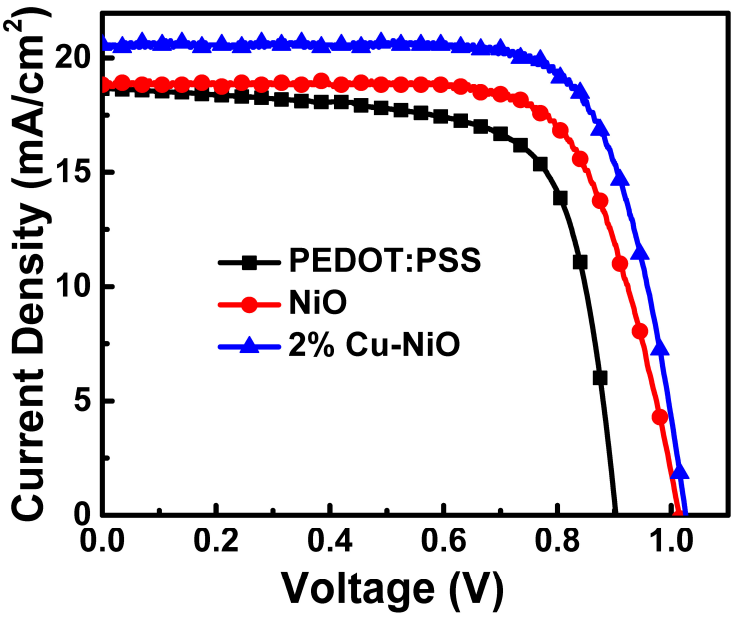

Figure 10. J-V characteristics of the devices made of PEDOT:PSS, NiO_x, and Cu-NiO_x as HTLs.

Table 3. Device performance of PEDOT:PSS, NiO_x, and Cu-NiO_x HTL PSCs (the average values were calculated from 12 devices for each HTL material).

HTL		V_{OC} (V)	J_{SC} (mA/cm^2)	Fill Factor	PCE (%)
PEDOT:PSS	Average	0.900 ± 0.020	17.919 ± 0.863	0.697 ± 0.015	11.239 ± 0.464
	Best	0.903	18.66	0.71	11.93
NiO	Average	1.015 ± 0.019	19.014 ± 0.456	0.702 ± 0.011	13.539 ± 0.239
	Best	1.015	18.83	0.71	13.72
2% Cu-NiO	Average	1.028 ± 0.003	20.172 ± 0.273	0.744 ± 0.005	15.417 ± 0.118
	Best	1.026	20.57	0.74	15.54

The EQE spectra of the PEDOT:PSS-, NiO_x-, and 2% Cu-NiO_x-based devices are displayed in Figure 11. The EQE spectra of NiO_x and Cu-NiO_x devices were similar, but the Cu-doped device exhibited a higher EQE value than the pristine NiO_x device did. A slight difference in EQE spectra at higher wavelengths for the PEDOT:PSS device was observed. The fabricated devices exhibited satisfactory EQE values in the entire visible region. The higher EQE values in the Cu-doped device indicated that Cu-NiO_x HTLs exhibited better charge transport properties.

The results of EIS performed on the fabricated devices are displayed in Figure 12. The Nyquist plot for the devices fabricated using PEDOT:PSS, NiO_x, and 2% Cu-NiO_x were analyzed in the frequency range from 10 Hz to 1 MHz, and the AC amplitude was 0.01 V under one solar illumination at a bias of V_{OC}. Typically, the higher-frequency regime corresponded to the charge transport resistance of the $MAPbI_3$/HTL interface and the lower-frequency regime was attributed to a low-frequency dielectric response of the perovskite materials [48,49]. A low impedance value is more favorable to carrier transport. The EIS results indicated that the Cu-NiO_x devices exhibited the lowest impedance value. This result was consistent with the J–V and EQE results.

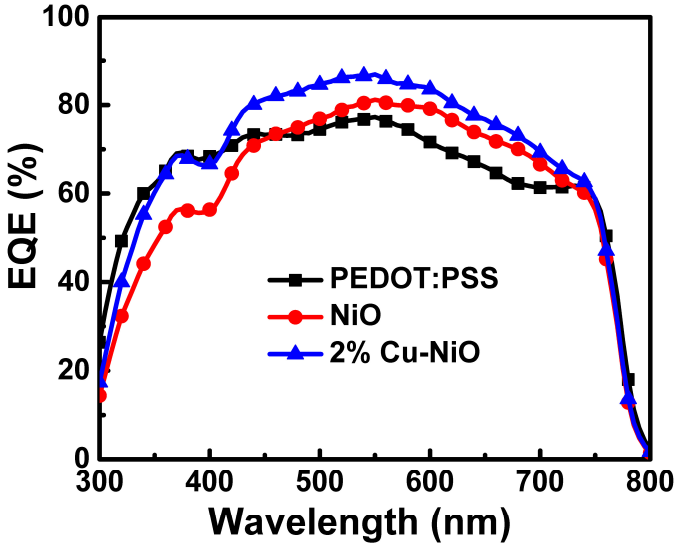

Figure 11. EQE of the devices made of PEDOT:PSS, NiO_x, and Cu-NiO_x as HTLs.

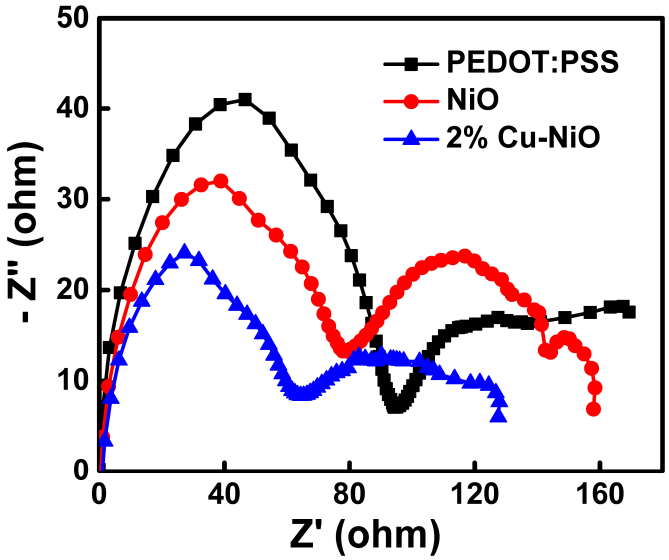

Figure 12. EIS of the devices made of PEDOT:PSS, NiO_x, and Cu-NiO_x as HTLs.

The Cu doping in NiO_x increased the electrical conductivity, which reduced the charge transport resistance at the $MAPbI_3$/HTL interface and enhanced the band alignment between perovskites and HTLs.

4. Conclusions

We fabricated inverted PSCs using NiO_x and Cu-NiO_x HTLs through spin-coating NP inks. The prepared spin-coated films were uniform and did not exhibit any voids. Cu incorporation into NiO_x did not change its crystalline nature and considerably improved its electrical conductivity. The optical bandgap decreased with an increase in the Cu concentration. Few nanoclusters occurred at higher doping concentrations because of the differences in the calcination temperature between $Ni(OH)_2$ and $Cu(OH)_2$. The Cu-NiO_x HTLs exhibited superior PL quenching and the least lifetime decay, which indicated that Cu-NiO_x exhibited superior charge transport compared with pristine NiO_x HTLs. The EQE in the Cu-doped device throughout the visible region was higher than that in other devices. EIS analysis revealed the incorporation of Cu in NiO_x HTL reduced the interface

impedance. The fabricated NiO_x and 2% Cu-NiO_x PSCs exhibited PCEs of 13.72% and 15.54%, respectively.

Author Contributions: Conceptualization, C.-H.T. and P.S.T.; methodology, C.-H.T., P.S.T. and C.-C.L.; validation, C.-H.T.; formal analysis, C.-H.T., P.S.T. and C.-C.L.; investigation, C.-H.T., P.S.T. and C.-C.L.; resources, C.-H.T.; data curation, C.-H.T., P.S.T. and C.-C.L.; writing—original draft preparation, C.-H.T. and P.S.T.; writing—review and editing, C.-H.T. and P.S.T.; supervision, C.-H.T.; project administration, C.-H.T.; funding acquisition, C.-H.T. All authors have read and agreed to the published version of the manuscript.

Funding: This research was funded by Ministry of Science and Technology (MOST) of Taiwan (grant No. MOST 108-2221-E-259-011).

Institutional Review Board Statement: Not applicable.

Informed Consent Statement: Not applicable.

Data Availability Statement: The data in this work are available on request from the corresponding author.

Conflicts of Interest: The authors declare no conflicts of interest.

References

1. Masri, M.; B, G.K.; Hezam, A.; Alkanad, K.; Prashantha, K.; Manjunath, S.H.; Udayabhanu; Masri, F.; Qahtan, T.F.; Byrappa, K. Metal Halide Perovskite-Based Photocatalysts for Organic Pollutants Degradation: Advances, Challenges, and Future Directions. *Colloids Surf. A Physicochem. Eng. Asp.* **2024**, *687*, 133387. [CrossRef]
2. Juhi, J.; Saski, M.; Kochaniec, M.K.; Wieczorek, W.; Dominko, R.; Lewiński, J. Exploring Metal Halide Perovskites as Active Architectures in Energy Storage Systems. *J. Mater. Chem. A* **2025**. [CrossRef]
3. Shooshtari, M.; Kim, S.-Y.; Pahlavan, S.; Rivera-Sierra, G.; Través, M.J.; Serrano-Gotarredona, T.; Bisquert, J.; Linares-Barranco, B. Advancing Logic Circuits with Halide Perovskite Memristors for Next-Generation Digital Systems. *SmartMat* **2025**, *6*, e70032. [CrossRef]
4. Afre, R.A.; Pugliese, D. Perovskite Solar Cells: A Review of the Latest Advances in Materials, Fabrication Techniques, and Stability Enhancement Strategies. *Micromachines* **2024**, *15*, 192. [CrossRef]
5. Liu, J.; Li, S.; Mei, A.; Han, H. Applications of Metal Oxide Charge Transport Layers in Perovskite Solar Cells. *Small Sci.* **2023**, *3*, 2300020. [CrossRef]
6. Wu, Y.-W.; Wang, C.-Y.; Yang, S.-H. Exploration and Optimization of the Polymer-Modified NiOx Hole Transport Layer for Fabricating Inverted Perovskite Solar Cells. *Nanomaterials* **2024**, *14*, 1054. [CrossRef]
7. Jeng, J.Y.; Chen, K.C.; Chiang, T.Y.; Lin, P.Y.; Tsai, T.D.; Chang, Y.C.; Guo, T.F.; Chen, P.; Wen, T.C.; Hsu, Y.J. Nickel Oxide Electrode Interlayer in $CH_3NH_3PbI_3$ Perovskite/PCBM Planar-Heterojunction Hybrid Solar Cells. *Adv. Mater.* **2014**, *26*, 4107–4113. [CrossRef]
8. Alghamdi, A.R.M.; Yanagida, M.; Shirai, Y.; Andersson, G.G.; Miyano, K. Surface Passivation of Sputtered NiO_x Using a SAM Interface Layer to Enhance the Performance of Perovskite Solar Cells. *ACS Omega* **2022**, *7*, 12147–12157. [CrossRef]
9. Zhu, K.; Chen, Y.; Wang, Y.; Feng, M.; Zhao, Y. Progress of Solution-Processed Metal Oxides as Charge Transport Layers towards Efficient and Stable Perovskite Solar Cells and Modules. *Mater. Today Nano* **2022**, *20*, 100252. [CrossRef]
10. Aristizábal-Duarte, L.; González-Hernández, M.; Reyes, S.E.; Ramírez-Rincón, J.A.; Ortiz, P.; Cortés, M.T. Enhanced Charge Transport in Inverted Perovskite Solar Cells via Electrodeposited La-Modified NiO_x Layers. *Energies* **2025**, *18*, 3590. [CrossRef]
11. Yuk, D.; Roe, J.; Lee, Y.; Kim, J.; Seo, J.; Yeop, J.; Song, T.; Kim, J.Y. Improving the Optoelectrical Properties of a Nickel Oxide Hole Transport Layer by Hydrogen Peroxide Treatment for Efficient Organic Solar Cells. *ACS Appl. Energy Mater.* **2024**, *7*, 4558–4564. [CrossRef]
12. Tang, G.; Chen, L.; Cao, X.; Wang, Y.; Zhang, H.; Tai, Q. A Review on Recent Advances in Flexible Perovskite Solar Cells. *Sol. RRL* **2025**, *9*, 2400844. [CrossRef]
13. Chang, C.-Y.; Wu, Y.-W.; Yang, S.-H.; Abdulhalim, I. Preparation of Nickel Oxide Nanoflakes for Carrier Extraction and Transport in Perovskite Solar Cells. *Nanomaterials* **2022**, *12*, 3336. [CrossRef] [PubMed]
14. Reyes, S.E.; González-Hernández, M.; Cortés, M.T.; Ortiz, P. Effect of NH_4F Surface Treatment of Electrodeposited NiOx on the Properties and Reproducibility of Inverted Perovskite Solar Cells. *Surf. Interfaces* **2025**, *56*, 105654. [CrossRef]
15. Lin, Y.; Zhang, X.; Zhong, X.; Lu, C.; Lu, Y.; Li, X.; Tu, S. Construction of Novel D-A Type Self-Assembled Molecules Together with NiOx for Flexible Perovskite Solar Cells. *Tetrahedron* **2025**, *176*, 134541. [CrossRef]

16. Noman, M.; Khan, Z.; Jan, S.T. A Comprehensive Review on the Advancements and Challenges in Perovskite Solar Cell Technology. *RSC Adv.* **2024**, *14*, 5085–5131. [CrossRef]
17. Tutundzic, M.; Zhang, X.; Lammar, S.; Singh, S.; Marchezi, P.; Merckx, T.; Aguirre, A.; Moons, E.; Aernouts, T.; Kuang, Y.; et al. Toward Efficient and Fully Scalable Sputtered NiO_x-Based Inverted Perovskite Solar Modules via Co-Ordinated Modification Strategies. *Sol. RRL* **2023**, *8*, 2300862. [CrossRef]
18. Kim, J.W.; Cho, E.; Lee, H.; Kwon, S.; Park, J.; Kim, M.; Kim, D.; Na, S.; Lee, S. Enhancing Efficiency of Inverted Perovskite Solar Cells by Sputtered Nickel Oxide Hole Transport Layers. *Sol. RRL* **2023**, *8*, 2300933. [CrossRef]
19. Yadav, K.; Samanta, A.; Ankita; Tarun; Das, S.; Kanjilal, A.; Pandey, U.K. Tailoring Sputter Grown NiOx Layer by Synergistic Surface Passivation for Efficient Perovskite Solar Cells. *Sol. Energy* **2025**, *288*, 113286. [CrossRef]
20. Feng, M.; Wang, Y.; Liu, F.; Ren, M.; Wang, H.; Guo, J.; Chen, Y.; Miao, Y.; Zhao, Y. Rational Buried Interface Engineering of Inorganic NiO_x Layer toward Efficient Inverted Perovskite Solar Cells. *Sol. RRL* **2023**, *8*, 2300712. [CrossRef]
21. Lu, X.; Fan, X.; Zhang, H.; Xu, Q.; Ijaz, M. Review on Preparation of Perovskite Solar Cells by Pulsed Laser Deposition. *Inorganics* **2024**, *12*, 128. [CrossRef]
22. Akalin, S.A.; Erol, M.; Uzunbayir, B.; Oguzlar, S.; Yildirim, S.; Choi, F.P.G.; Gunes, S.; Menda, U.D.Y.; Mendes, M.J. Physically-Deposited Hole Transporters in Perovskite PV: NiO_x Improved with Li/Mg Doping. *Adv. Mater. Technol.* **2024**, *9*, 2301760. [CrossRef]
23. Jiang, Q.; Zhu, K. Rapid Advances Enabling High-Performance Inverted Perovskite Solar Cells. *Nat. Rev. Mater.* **2024**, *9*, 399–419. [CrossRef]
24. Mann, D.S.; Kwon, S.-N.; Patil, P.; Na, S.-I. Revivification of Nickel Oxide-Perovskite Interfaces via Nickel Nitrate to Boost Performance in Perovskite Solar Cells. *Nano Energy* **2022**, *106*, 108062. [CrossRef]
25. Song, D.; Shin, S.W.; Wu, H.-P.; Diau, E.W.-G.; Correa-Baena, J.P. Toward Maximizing Hole Selection with Self-Assembled Monolayers in Sn-Based Perovskite Solar Cells. *ACS Energy Lett.* **2025**, *10*, 1292–1312. [CrossRef]
26. Soopy, A.K.K.; Parida, B.; Aravindh, S.A.; Al Ghaithi, A.O.; Qamhieh, N.; Amrane, N.; Benkraouda, M.; Liu, S.; Najar, A. Towards High Performance: Solution-Processed Perovskite Solar Cells with Cu-Doped $CH_3NH_3PbI_3$. *Nanomaterials* **2024**, *14*, 172. [CrossRef]
27. Verma, A.P.; Yadav, P.; Nalwa, K.S.; Kumar, M. Interface Engineering and Band Alignment Studies of Cu Doped NiO as a Hole Transport Layer for Triple Cationic Perovskite Solar Cells. *Small* **2025**, *21*, 2504237. [CrossRef]
28. Jin, Y.; Feng, H.; Li, Y.; Zhang, H.; Chen, X.; Zhong, Y.; Zeng, Q.; Huang, J.; Weng, Y.; Yang, J.; et al. Recrystallizing Sputtered NiO_x for Improved Hole Extraction in Perovskite/Silicon Tandem Solar Cells. *Adv. Energy Mater.* **2024**, *15*, 2403911. [CrossRef]
29. Yu, S.; Xiong, Z.; Zhou, H.; Zhang, Q.; Wang, Z.; Ma, F.; Qu, Z.; Zhao, Y.; Chu, X.; Zhang, X.; et al. Homogenized NiOx Nanoparticles for Improved Hole Transport in Inverted Perovskite Solar Cells. *Science* **2023**, *382*, 1399–1404. [CrossRef]
30. Wang, L.; Li, Y.; Shen, H.; Wang, L.; Zhao, Q.; Zheng, J.; Li, H.; Xie, Z.; Chen, A.; Miao, S.; et al. Highly Stable Inverted Perovskite Solar Cells with All-Inorganic Selective Contact Using Iron-Doped Zinc Oxide. *J. Chem. Phys.* **2025**, *162*, 094703. [CrossRef]
31. Li, M.; Zhang, Z.; Sun, J.; Liu, F.; Chen, J.; Ding, L.; Chen, C. Perovskite Solar Cells with NiO_x Hole-Transport Layer. *J. Semicond.* **2023**, *44*, 100201. [CrossRef]
32. Valenzuela-López, J.Y.; Millán-Franco, M.A.; Suárez-Campos, G.; Camacho-Cáceres, J.; Rodríguez-Castañeda, C.A.; Moreno-Romero, P.M.; Torres-Herrera, D.M.; Sotelo-Lerma, M.; Hu, H. Influence of Nickel Precursor Solutions on Nickel Oxide Thin Film Formation and Photovoltaic Properties of Air-Processed Inverted Perovskite Solar Cells. *Opt. Mater.* **2024**, *149*, 115082. [CrossRef]
33. Madani, S.; Tesfamichael, T.; Wang, H.; Motta, N. Study of Pb-Based and Pb-Free Perovskite Solar Cells Using Cu-Doped $Ni_{1-X}O$ Thin Films as Hole Transport Material. *Ceram. Int.* **2022**, *48*, 15207–15217. [CrossRef]
34. Liu, S.; Biju, V.P.; Qi, Y.; Chen, W.; Liu, Z. Recent Progress in the Development of High-Efficiency Inverted Perovskite Solar Cells. *NPG Asia Mater.* **2023**, *15*, 27. [CrossRef]
35. Luo, X.; Liu, X.; Lin, X.; Wu, T.; Wang, Y.; Han, Q.; Wu, Y.; Segawa, H.; Han, L. Recent Advances of Inverted Perovskite Solar Cells. *ACS Energy Lett.* **2024**, *9*, 1487–1506. [CrossRef]
36. Andrade, P.H.M.; Volkringer, C.; Loiseau, T.; Tejeda, A.; Hureau, M.; Moissette, A. Band Gap Analysis in MOF Materials: Distinguishing Direct and Indirect Transitions Using UV–Vis Spectroscopy. *Appl. Mater. Today* **2024**, *37*, 102094. [CrossRef]
37. Barkaoui, S.; Wang, Y.; Zhang, Y.; Gu, X.; Li, Z.; Wang, B.; Baiker, A.; Li, G.; Zhao, Z. Critical Role of NiO Support Morphology for High Activity of Au/NiO Nanocatalysts in CO Oxidation. *iScience* **2024**, *27*, 110255. [CrossRef]
38. de Souza Caldas, L.; Prieto, M.J.; Tănase, L.C.; Tiwari, A.; Schmidt, T.; Cuenya, B.R. Correlative in Situ Spectro-Microscopy of Supported Single CuO Nanoparticles: Unveiling the Relationships between Morphology and Chemical State during Thermal Reduction. *ACS Nano* **2024**, *18*, 13714–13725. [CrossRef]
39. Baraneedharan, P.; Sekar, S.; Murugesan, S.; Ahamada, D.; Mohamed, S.A.B.; Lee, Y.; Lee, S. Recent Advances and Remaining Challenges in Perovskite Solar Cell Components for Innovative Photovoltaics. *Nanomaterials* **2024**, *14*, 1867. [CrossRef]
40. Zhang, W.; Shen, H.; Zhang, J.; Zhang, J.; Lu, L.; Zhu, X.; Li, D. NiO_x Thickness Dependent Improvement of NiO_x/Perovskite Interface for Inverted Planar Perovskite Solar Cells. *Opt. Mater.* **2022**, *132*, 112774. [CrossRef]

41. Chen, P.; Xiao, Y.; Li, S.; Jia, X.; Luo, D.; Zhang, W.; Snaith, H.J.; Gong, Q.; Zhu, R. The Promise and Challenges of Inverted Perovskite Solar Cells. *Chem. Rev.* **2024**, *124*, 10623–10700. [CrossRef]
42. Ye, Z.; Xia, J.; Zhang, D.; Duan, X.; Xing, Z.; Jin, G.; Cai, Y.; Xing, G.; Chen, J.; Ma, D. Efficient Quasi-2D Perovskite Light-Emitting Diodes Enabled by Regulating Phase Distribution with a Fluorinated Organic Cation. *Nanomaterials* **2022**, *12*, 3495. [CrossRef]
43. Miah, M.H.; Khandaker, M.U.; Aminul Islam, M.; Nur-E-Alam, M.; Osman, H.; Ullah, M.H. Perovskite Materials in X-Ray Detection and Imaging: Recent Progress, Challenges, and Future Prospects. *RSC Adv.* **2024**, *14*, 6656–6698. [CrossRef]
44. Chen, W.; Wu, Y.; Fan, J.; Djurišić, A.B.; Liu, F.; Tam, H.W.; Ng, A.; Surya, C.; Chan, W.K.; Wang, D.; et al. Understanding the Doping Effect on NiO: Toward High-Performance Inverted Perovskite Solar Cells. *Adv. Energy Mater.* **2018**, *8*, 1703519. [CrossRef]
45. Nyiekaa, E.A.; Aika, T.A.; Orukpe, P.E.; Akhabue, C.E.; Danladi, E. Development on Inverted Perovskite Solar Cells: A Review. *Heliyon* **2024**, *10*, e24689. [CrossRef] [PubMed]
46. Diethelm, M.; Lukas, T.; Smith, J.; Dasgupta, A.; Caprioglio, P.; Futscher, M.; Hany, R.; Snaith, H.J. Probing Ionic Conductivity and Electric Field Screening in Perovskite Solar Cells: A Novel Exploration through Ion Drift Currents. *Energy Environ. Sci.* **2025**, *18*, 1385–1397. [CrossRef] [PubMed]
47. Aliyaselvam, O.V.; Mustafa, A.N.; Azam, M.A.; Chelvanathan, P.; Islam, M.A.; Mahalingam, S.; Arith, F. Unveiling the Prospect of Copper Iodide as Hole Transporting Layer in Perovskite Solar Cell by Selective Dopant Strategy: A Review. *Mater. Sci. Semicond. Process.* **2025**, *197*, 109679. [CrossRef]
48. Chin, Y.-C.; Daboczi, M.; Henderson, C.; Luke, J.; Kim, J.-S. Suppressing PEDOT:PSS Doping-Induced Interfacial Recombination Loss in Perovskite Solar Cells. *ACS Energy Lett.* **2022**, *7*, 560–568. [CrossRef]
49. Qu, J.; Zhang, W.; Chen, Y.; Zhao, H.; Wei, Y.; Zhou, R.; Wan, H.; Deng, J.; Fan, D.; Luo, Y.; et al. Multifunctional Amine Salt Additive for Enhancing the Performance of Perovskite and Perovskite/Silicon Tandem Solar Cells. *Chem. Eng. J.* **2025**, *515*, 163967. [CrossRef]

Disclaimer/Publisher's Note: The statements, opinions and data contained in all publications are solely those of the individual author(s) and contributor(s) and not of MDPI and/or the editor(s). MDPI and/or the editor(s) disclaim responsibility for any injury to people or property resulting from any ideas, methods, instructions or products referred to in the content.